Seismic Behavior of Piled Raft under Moderate and Strong Earthquakes Based on Observation and Numerical Simulation

観測および数値シミュレーションに基づくパイルド・ラフトの中地震および大地震時の挙動

Kiyoshi Yamashita 山下 清*1 Junji Hamada 濱田 純次*2
Yoshimasa Shigeno 重野 喜政*3 Tomohiro Tanikawa 谷川 友浩*4

Summary

The seismic behavior of a piled raft foundation with cement deep mixing walls (DMWs) in soft ground was investigated based on the observation results of the 2011 Tohoku Earthquake. The results were examined focusing the effects of inertial force from the structure and action of ground movements on the foundation system. Furthermore, the seismic performance under strong earthquakes was also discussed using the previous 3D finite element (FE) analysis results. Consequently, it was found in soft ground that the bending moment near the pile head were affected mainly by the lateral ground deformation, rather than the shear force resulted from the structure inertial force. It was also found that the DMWs restrained the amplification of ground deformation in the grids and this would lead to the significant decrease in bending moment near the pile head.

Keywords: piled raft foundation, grid-form deep mixing walls, seismic loading, monitoring

梗　概

深層混合処理による格子状地盤改良を併用した軟弱地盤上のパイルド・ラフト基礎について，2011年東北地方太平洋沖地震時の観測結果に基づき，地震時に生じる杭の応力に及ぼす建物慣性力と地盤変形の影響に焦点をあてて考察した。さらに，既往の3次元FEMによるシミュレーション解析に基づき，大地震時のパイルド・ラフト基礎の挙動についても考察した。その結果，軟弱地盤では杭頭付近の曲げモーメントは主に地盤の水平変位により生じ，構造物の慣性力に伴うせん断力の影響は小さいこと，杭の曲げモーメントは格子状改良体が地盤変形を抑えることにより大幅に低減することが示された。

キーワード：パイルド・ラフト基礎，格子状地盤改良，地震荷重，挙動観測

1 INTRODUCTION

In recent years, the effectiveness of piled rafts in reducing average and differential settements has been confirmed not only on favorable ground conditions as shown by Katzenbach et al. (2000), Poulos (2001) and Mandolini et al. (2005), but also on unfavorable ground conditions with ground improvement techniques (Yamashita et al., 2011a; Yamashita et al., 2011b). Piled rafts can provide sufficient capacities against lateral and moment loads from the structure because the loads are carried by both the piles and raft. It has become necessary to develop more reliable seismic design methods for piled raft foundations, particularly in highly seismic areas such as Japan. However, case histories on monitoring seismic soil-pile-structure interaction of full-scale piled rafts are very limited (Mendoza et al., 2000; Hamada et al., 2015; Yamashita et al., 2016). Yamashita et al. (2012) have reported the seismic response of a piled raft with the grid-form deep cement mixing walls (DMWs) supporting a 12-story residential building at the time of the 2011 off the Pacific coast of Tohoku Earthquake (the 2011 Tohoku Earthquake).

＊1 Executive Manager, Research & Development Institute, Dr. Eng. 技術研究所 専門役 博士(工学)
＊2 Group Leader, Research & Development Institute, Dr. Eng. 技術研究所 地盤・基礎部 基礎構造グループ長 博士(工学)
＊3 Group Leader, Research & Development Institute 技術研究所 構造部 応用数理グループ長
＊4 Associate Chief Researcher, Research & Development Institute 技術研究所 地盤・基礎部 研究主任

This paper presents static and seismic behavior of the piled raft system supporting the 12-story building. In order to understand real seismic behavior of the piled raft in soft ground, the static and dynamic monitoring results are examined focusing the effects of inertial force from the structure and action of ground movements on the foundation system. Furthermore, based on the previous results of the numerical simulation analysis, the seismic performance of the foundation system under strong earthquakes was also discussed.

2 STRUCTURE

2.1 Soil conditions and foundation design

The 12-story residential building is located in Toyo, Tokyo. The building is a reinforced concrete structure with a base isolation system of laminated rubber bearings; it was completed in 2008. Figure 1 shows a schematic view of the building and the foundation with a typical soil profile. The subsoil consists of an alluvial stratum to a depth of 44 m, underlain by a diluvial sand-and-gravel layer of SPT *N*-values of 60 or higher. The ground water table appears approximately 1.8 m below the ground surface.

The total load in the structural design was 198.8 MN, which corresponds to the sum of the dead load and the live load. The average contact pressure over the raft was 199 kPa. To improve the bearing capacity of the silty soil beneath the raft, as well as to cope with the liquefiable silty sand between depths of 3 and 7 m below the ground surface, the grid-form deep mixing walls were constructed to a depth of 16 m with the bottom being embedded in the stiffer silty clay with an undrained shear strength of 75 kPa (OCR of 2 or higher). The spacing between the walls was about 6 to 9 m and the improvement area ratio (ratio of improved area in plan to raft area) was 0.25. The design standard strength of the stabilized soil was 1.8 MPa.

Furthermore, to reduce the settlement to acceptable levels, sixteen 45-m-long piles, 0.8-1.2 m in diameter, were used. The pile toes reached the very dense sand-and-gravel layer sufficiently well enough to ensure the toe resistance. The piles consisted of steel pipe-concrete composite (SC) piles in the top portion and pre-tensioned spun high-strength concrete (PHC) piles in the bottom portion. The piles were constructed by inserting four sets of pile segments (one SC pile and three PHC piles) into a pre-augered borehole filled with mixed-in-place soil cement slurry. Figure 2 shows the layout of the piles and the grid-form deep cement mixing walls.

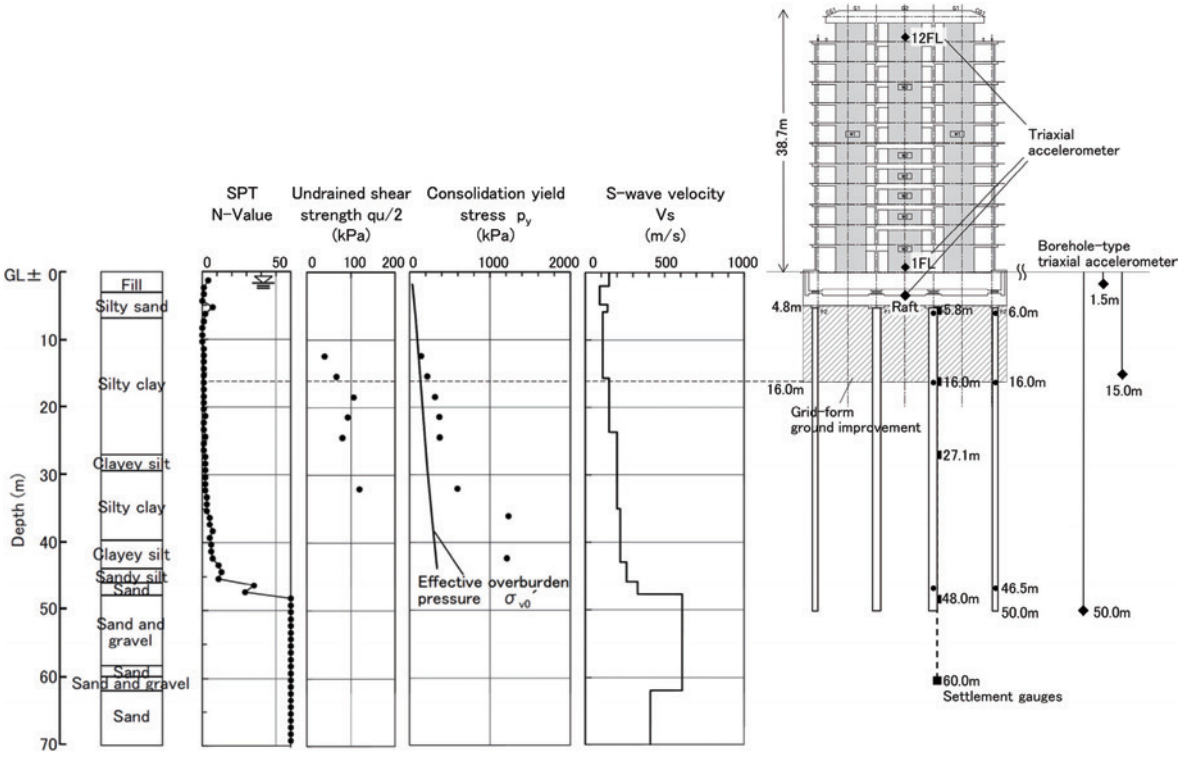

Fig. 1 Schematic view of the building and foundation with soil profile

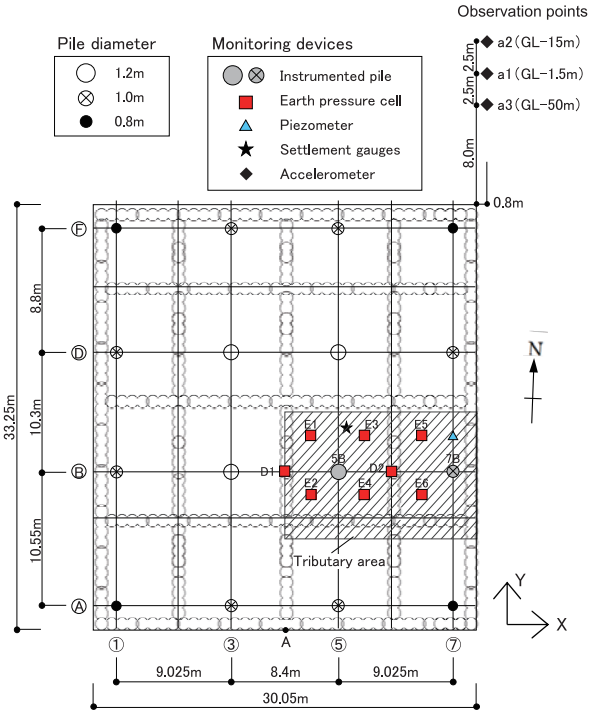

Fig. 2 Layout of piles and grid-form deep mixing walls with locations of monitoring devices

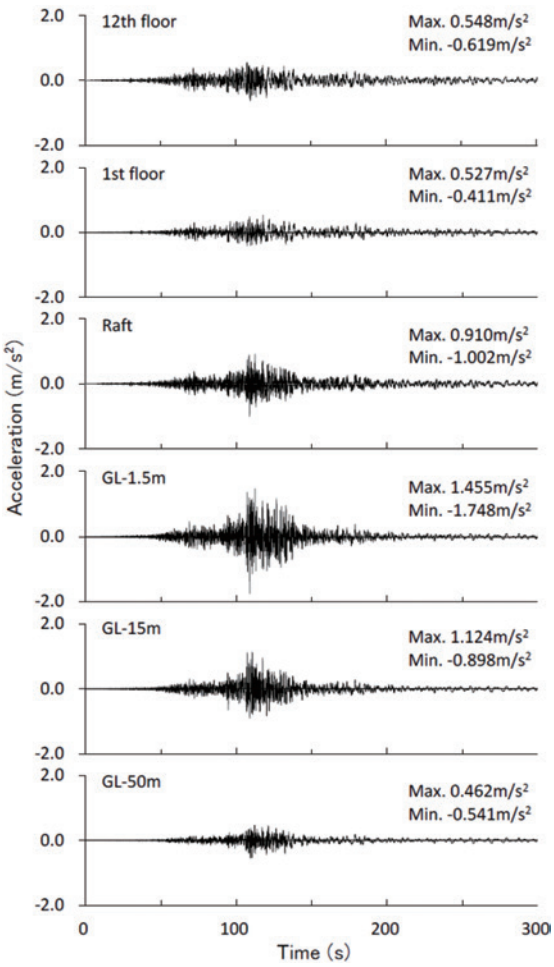

Fig. 3 Time histories of EW accelerations of ground and structure

2.2 Instrumentation

The locations of the monitoring devices are shown in Fig. 2. Two piles, 5B and 7B, were provided with a couple of LVDT-type strain gauges at depths of 6.0 m (near the pile head), 16.0 m and 46.5 m (near the pile toe) from the ground surface. Near the instrumented piles, eight earth pressure cells and one piezometer were installed beneath the raft at a depth of 4.8 m. Six earth pressure cells, E1-E6, were installed on the intact soil, and two earth pressure cells, D1 and D2, were installed on the top surface of the deep mixing walls. The vertical ground displacements below the raft were measured by differential settlement gauge (LVDT). As for the monitoring of the seismic response of the ground, a vertical array consisting of borehole-type triaxial servo accelerometers (a1, a2 and a3 in Fig. 2) was installed at depths of 1.5 m, 15.0 m and 50.0 m below the ground surface to record the north-south (NS), east-west (EW) and up-down (UD) accelerations of the ground. The accelerometers are located 8-13 m apart from the north-east corner of the building. As for the seismic response of the structure, triaxial servo accelerometers were installed on the first and the 12th floors and the raft as shown in Fig. 1. Further details in soil conditions, foundation design and instrumentation are described in Yamashita et al. (2012).

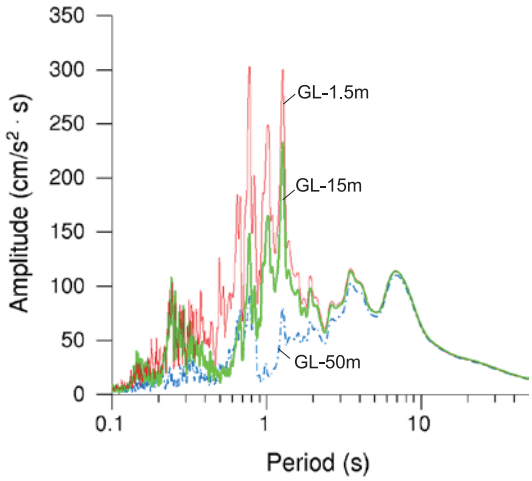

Fig. 4 Fourier spectra of EW ground accelerations

3 RESULTS OF SEISMIC MONITORING

The 2011 Tohoku earthquake, with an estimated magnitude of M_w= 9.0 on the Moment Magnitude Scale, struck East Japan

on March 11, 2011. According to the JMA (Japan Meteorological Agency), an earthquake epicenter was located about 130 km east-southeast off the Oshika Peninsura at a depth of 23.7 km. The distance from the epicenter to the building site was about 380 km.

Figure 3 shows the time histories of the EW accelerations of the ground and the structure. A peak horizontal ground acceleration of 1.75 m/s^2 was observed near the ground surface. Figure 4 shows the Fourier spectra of the EW accelerations of the ground motion and those of the structure response, which were smoothed by 0.05 Hz Parzen window. As to the accelerations near the ground surface, it can be seen that components of the periods of 0.7, 1.0 and 1.2 s were predominant.

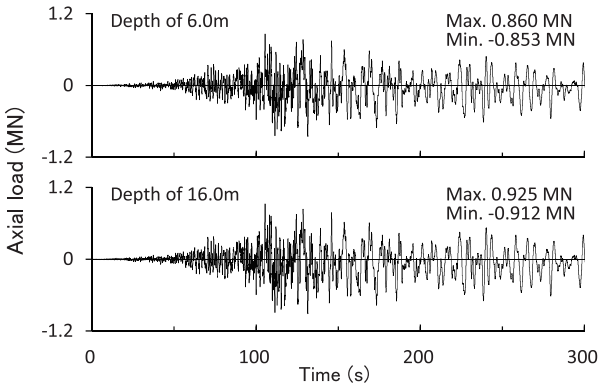

(a) Pile 5B

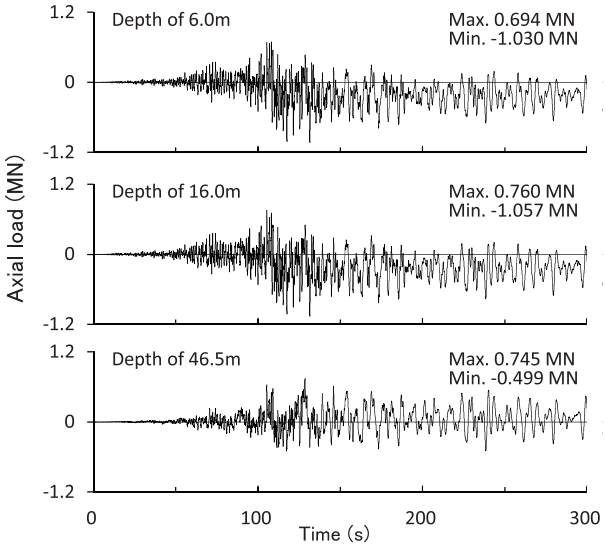

(b) Pile 7B

Fig. 5 Increments of axial loads of piles

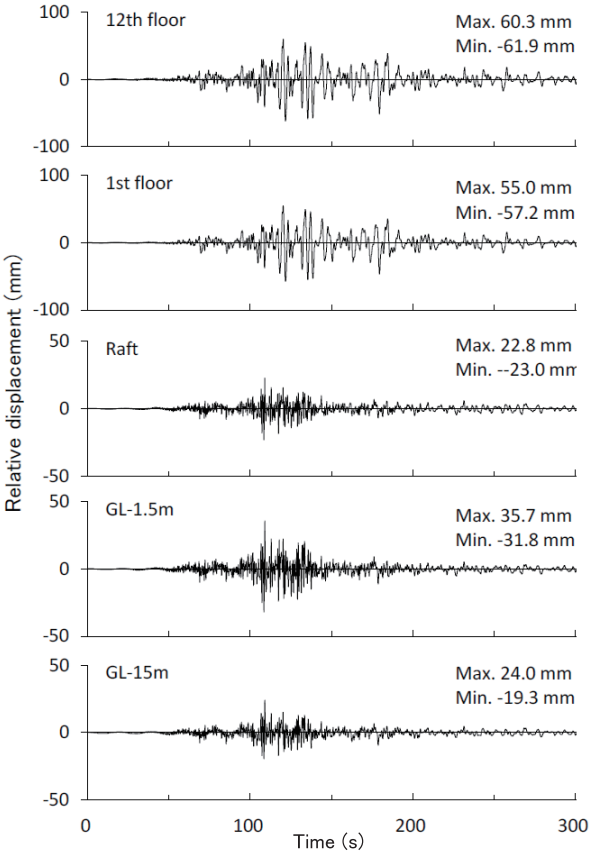

Fig. 6 Time histories of relative ground and structure displacements in EW direction

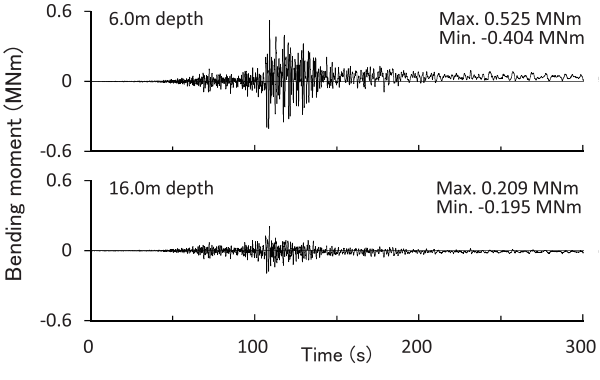

(a) Pile 5B

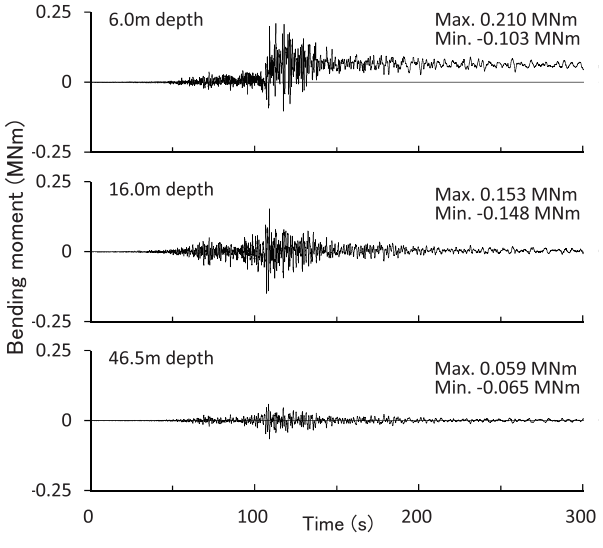

(b) Pile 7B

Fig. 7 Time histories of pile bending moment (EW)

Figure 5 shows the time histories of the increments in axial loads of the piles. The maximum amplitude for Pile 5B near the pile head was 860 kN in compression and 853 kN in tension, while that for Pile 7B near the pile head was 694 kN in compression and 1030 kN in tension. The largest amplitudes of axial load occurred at intermediate depths for both piles. Furthermore, the ratio of the load amplitude near the pile toe to that near the pile head was 1.07 in compression and 0.48 in tension, which is considerably larger than the ratio of the pile-toe load to the pile-head load in the static measurements. Figure 6 shows the time histories of the relative displacement between the ground (or structure) and that at a depth of 50 m in the EW direction. The displacements were calculated by the double integration of the acceleration records, for which low-frequency components less than 0.05 Hz were removed. Figure 7 shows the time histories for the bending moments of Piles 5B and 7B, respectively. The maximum bending moments near the pile head in the EW direction were 525 and 210 kNm for Piles 5B and 7B, respectively. The maximum bending moment at the intermediate depth (at 16 m depth) were 209 and 153 kNm, respectively, which were not so small compared to those near the pile head.

4 DYNAMIC SOIL-STRUCTURE INTERACTION IN PILED RAFT SYSTEM

4.1 Influence of seismic action on foundation

Seismic action will induce additional lateral forces in the structure and also induce lateral motions in the ground supporting the structure. These can be induced in the foundation system via two mechanisms (Poulos, 2016):

_Inertial forces and the consequent overturning moments developed by the lateral excitation of the structure

_Kinematic forces acting on the raft and piles induced by the action of ground movements

Figure 8 illustrates the influence of seismic action on a piled raft embedded in soft ground. In the following, the effects of the action of ground movements as well as the inertial forces from the structure on the piled raft system were examined based on the seismic monitoring results.

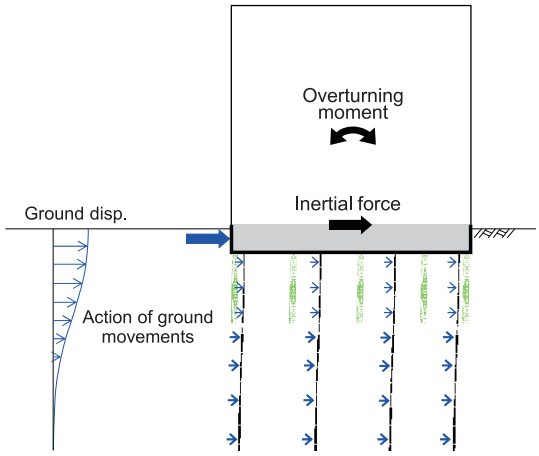

Fig. 8 Influence of seismic action on piled raft embedded in soft ground

4.2 Effects of inertial force from structure on pile bending moment

Figure 9 shows the time histories of the bending moment in the piles during 105-120 s. Figure 10 shows the relation of the bending moment near pile head with those at 16 and 46.5 m depth (near the pile toe). The bending moments at depths of 6 and 16 m were in phase both for Piles 5B and 7B, while the bending moment at 46.5 m depth in Pile 7B was out of phase and a negative correlation between them is seen in Fig. 10(b).

Figure 11 shows the time history of the inertial forces from the structure in the EW direction during 105-125 s including the peak responses. The inertial forces were estimated using the mass in structural design and the accelerations observed on the raft, the first and twelfth floors shown in Fig. 3. The weight of the superstructure above the seismic isolators and that of the raft are 152 and 41 MN, respectively (Hamada et al., 2014). Although the mass of the superstructure is much greater than that of the raft, the estimated peaks of the superstructure inertial force were slightly greater than those of

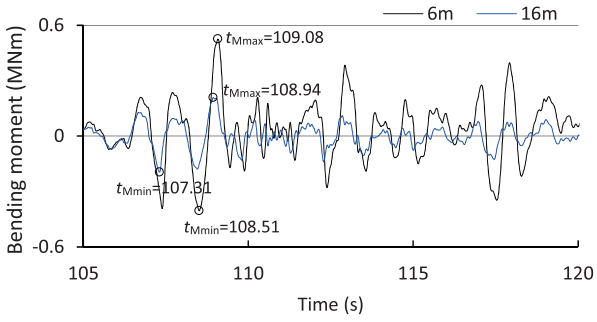

(a) Pile 5B (6 and 16 m depths)

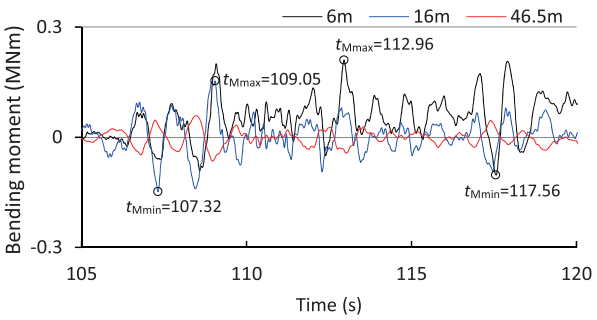

(b) Pile 7B (6, 16 and 46.5 m depths)

Fig. 9 Time histories of pile bending moment (EW)

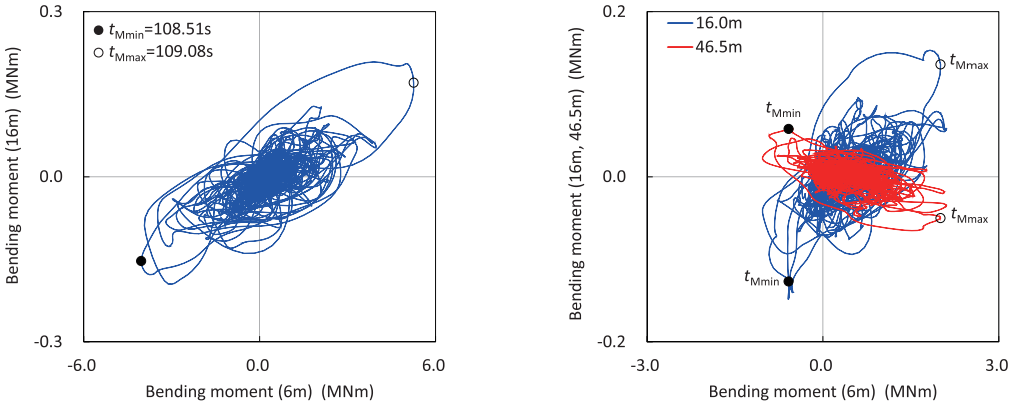

(a) Pile 5B (b) Pile 7B

Fig. 10 Bending moment (6 m depth) vs. bending moment (16 and 46.5 m depths)

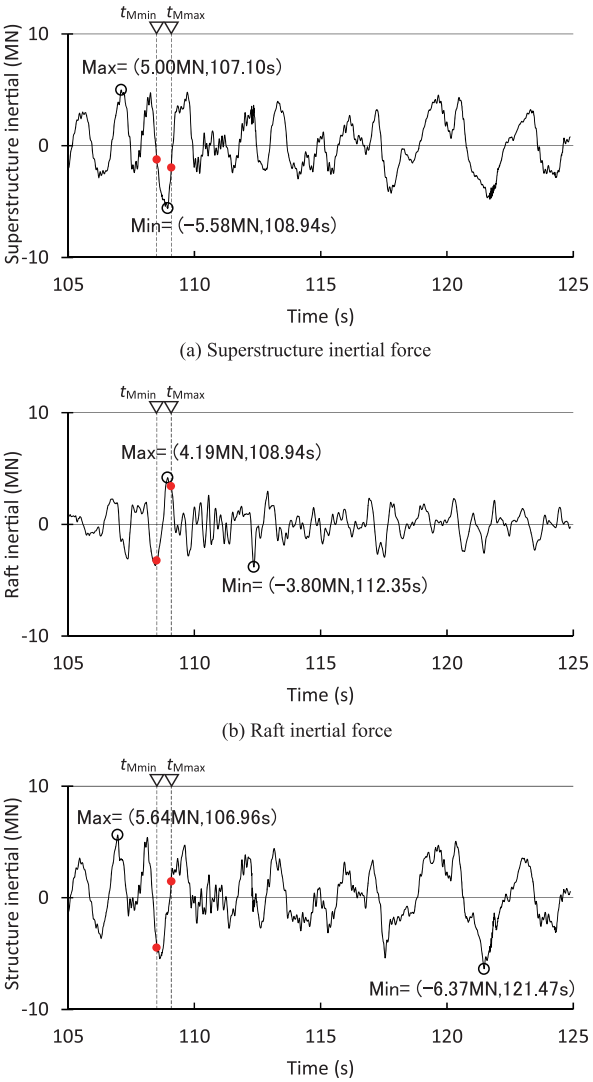

(a) Superstructure inertial force

(b) Raft inertial force

(c) Structure inertial force

Fig. 11 Time histories of inertial forces (EW)

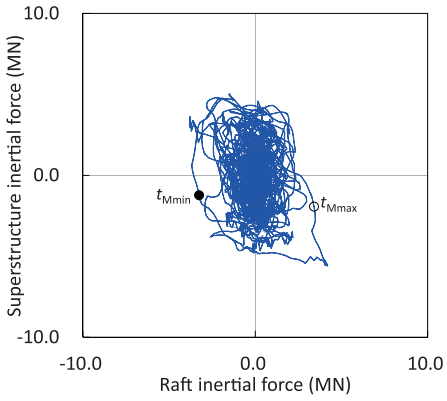

Fig. 12 Raft inertial force vs. superstructure inertial force

the raft inertial force due to the base isolation system. As indicated by the red circles in Fig. 11, the superstructure inertial force was out of phase with the raft inertial force and also with the structure inertial force (which means the sum of the superstructure and raft inertial forces) when the bending moment near the pile head (5B) was at its maximum (t_{Mmax} = 109.08 s) shown in Fig. 9(a). However, when the bending moment was at its minimum (t_{Mmin} = 108.51 s), the superstructure inertial force was in phase with both the raft and structure inertial forces. The relation of the raft inertial force with the superstructure inertial force (during 0-150 s) is shown in Fig. 12. There appears to be a negative correlation between them and both the inertial forces tend to cancel each other. As a result, the peaks of the structure inertial force was comparable with those of the superstructure inertial force.

Figure 13 shows the relations of the inertial force with the bending moment near the pile head (5B). It is seen that the superstructure inertial force had no significant correlation with the bending moment. On the other hand, the raft inertial force was in phase with the bending moment, and generated 81 and 86% of its maximum and minimum at $t = t_{Mmax}$ and t_{Mmin}, respectively. This arises because the behavior of the embedded raft (i.e., the raft inertial force) would be affected significantly by the ground displacements near the surface which had strong correlation with the bending moment (as shown in Fig. 14(a)). The maximum amplitude of the structure inertial force was -4.5

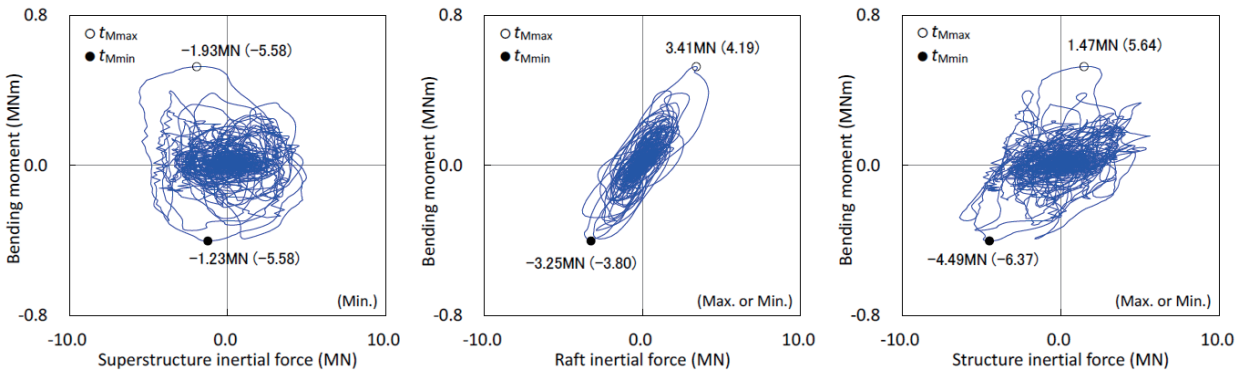

(a) Superstructure inertial force (b) Raft inertial force (c) Structure inertial force

Fig. 13 Inertial force vs. bending moment near pile head in Pile 5B (EW)

MN at $t = t_{Mmin}$ and generated 70% of its minimum as shown in Fig. 13(c). Thus, the effect of the structure inertial force on the bending moment was not necessarily significant.

4.3 Effects of ground movements on pile bending moment

Figure 14 shows the relations of the ground displacement with the bending moment. The bending moments near the pile head in both the piles had strong correlation with the ground displacements near the surface. Furthermore, the bending moments at 16 m depth had significant correlation with the ground displacements at 15 m depth. The relations of the raft displacement with the bending moment near the pile head are shown in Fig. 15. It is seen that the bending moment near the pile head had strong correlation with the raft displacement (which is approximately equal to the ground displacement just below the raft bottom at 4.8 m depth) for both the piles.

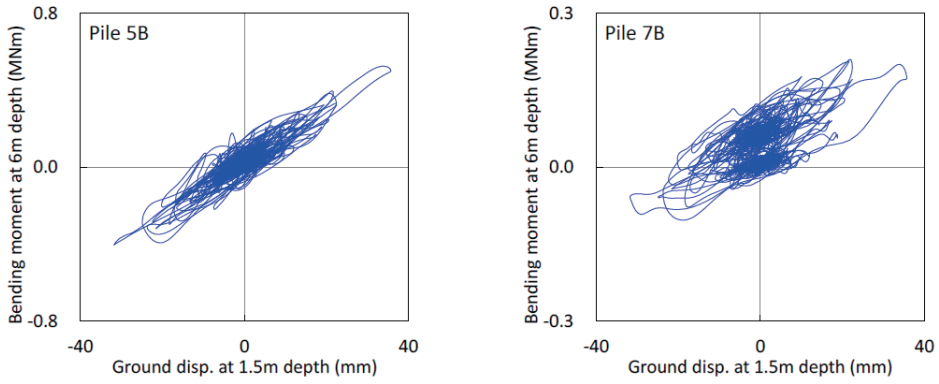

(a) Ground disp. at 1.5 m depth vs. bending moment at 6 m depth

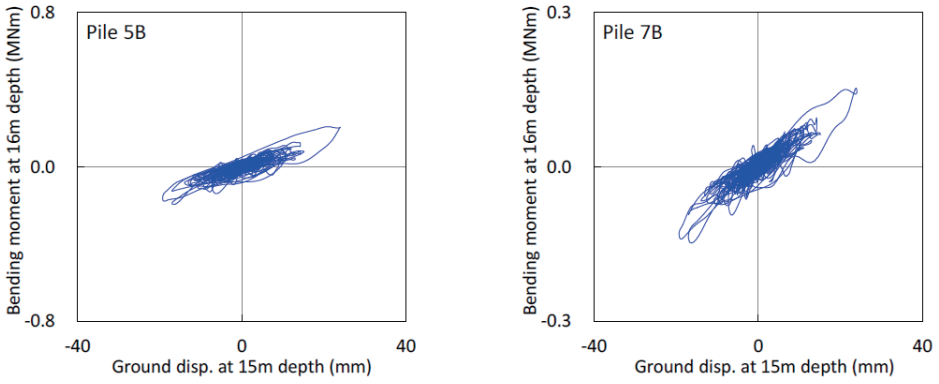

(b) Ground disp. at 15 m depth vs. bending moment at 16 m depth

Fig. 14 Ground displacement at 1.5 and 15 m depths vs. bending moment at 6 and 16 m depths (EW)

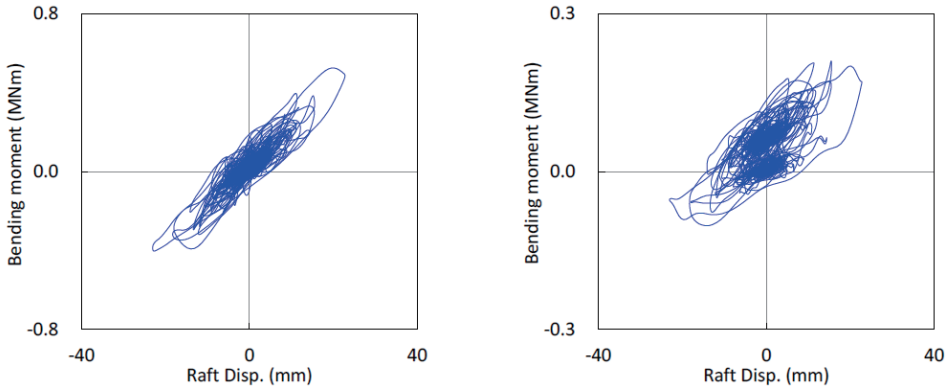

(a) Pile 5B (b) Pile 7B

Fig. 15 Raft displacement vs. bending moment at 6 m depth (EW)

Figure 16 shows the time histories of the ground displacements at 1.5 and 15 m depths and the raft displacement relative to the ground displacement at 50 m depth during 105-120 s including the maximum and minimum responses. It is seen that all the displacement histories were almost in phase. Figure 17(a) shows the relation of the ground displacement at 1.5 m depth with that at 15 m depth. The ground displacement at 1.5 m depth had strong correlation with that at 15 m depth, but the amplitude of the former was considerably greater than that of the latter. Namely, the ground displacement near the surface was about 1.5 times amplified from that at 15 m depth. Figure 17(b) shows the relation of the ground displacement at 1.5 m depth with the raft displacement. The ground displacement near the surface had strong correlation also with the raft displacement, while the amplitude of the former was considerably greater than that of the latter. Figure 18 shows the relation of the ground displacement at 15 m depth with the raft displacement. It is seen that the raft displacement was in phase with the ground displacement at 15 m depth and both the amplitudes were almost identical. This indicates that the DMWs, whose bottom reached relatively stiff clay below the depth of 15.7 m, restrained the amplification of the lateral ground displacements in the DMW grids.

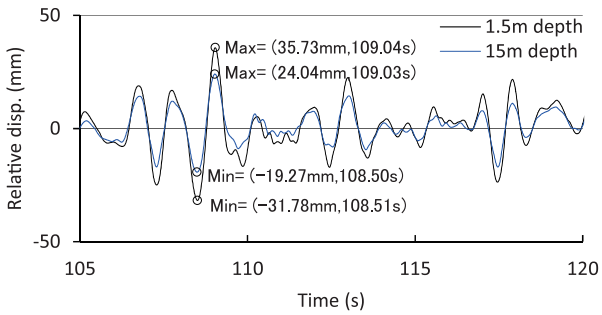

(a) Ground displacements (1.5 and 15 m depths)

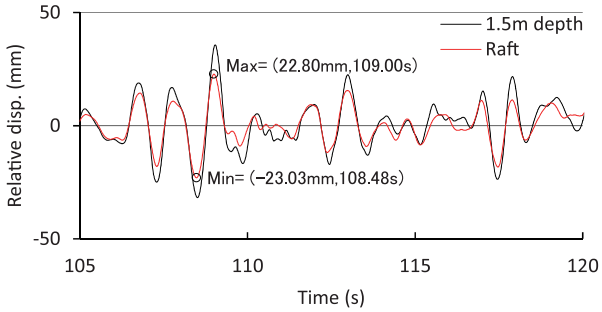

(b) Ground (1.5 m depth) and raft displacements

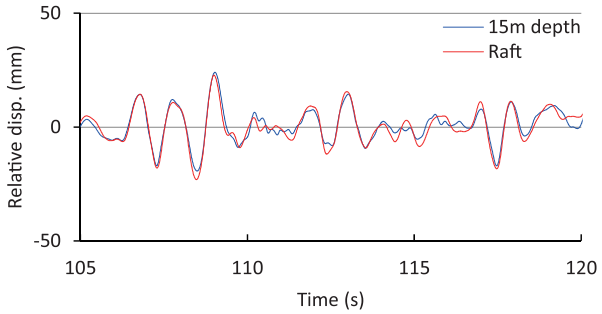

(c) Ground (15 m depth) and raft displacements

Fig. 16 Time histories of relative ground displacement and raft displacement (EW)

Figure 19 shows the relations of the relative displacement (δS - δR) with the bending moment near the pile head (5B and 7B), where δS and δR mean the ground displacement near the surface and raft displacement, respectively. Tamura and Hida (2014) have pointed out based on the dynamic centrifuge tests on a superstructure-footing model in sand that the peaks of dynamic earth pressure acting on the side of the embedded pile cap increased concurrently with the relative displacement between the pile cap and the soil. Figure 19 suggests that the bending moments near the pile head have significant correlation with the dynamic earth pressure acting on the raft side. Figure 20 shows the relation of the structure inertial force with the relative displacement (δS - δR). Although there appears to be no significant correlation between them, the relative displacement at $t = t_{\mathrm{Mmax}}$ or t_{Mmin} was in phase with the

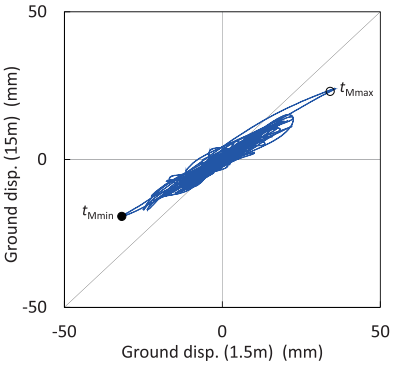

(a) Ground disp. (1.5m) vs. ground disp. (15m)

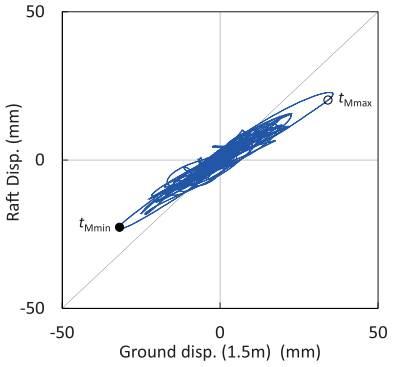

(b) Ground disp. (1.5m) vs. raft disp.

Fig. 17 Ground displacement at 1.5 m depth vs. ground displacement at 15 m depth and raft displacement (EW)

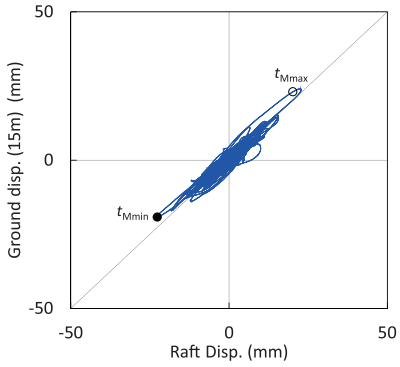

Fig. 18 Relation of raft displacement with ground displacement at 15 m depth (EW)

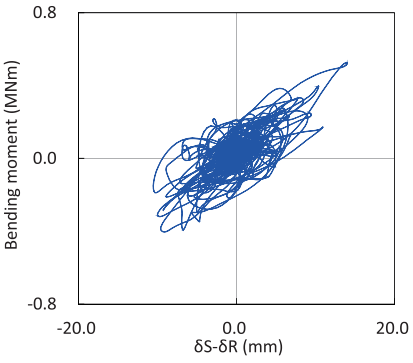

(a) Pile 5B

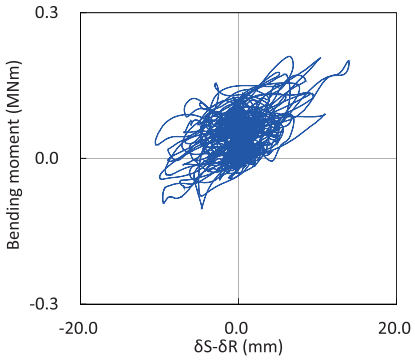

(b) Pile 7B

Fig. 19 Relative displacement (δ*S*-δ*R*) vs. bending moment near pile head (EW)

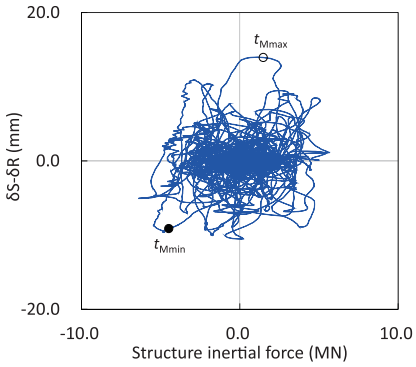

Fig. 20 Structure inertial force vs. relative displacement (δ*S*-δ*R*)

structure inertial force. Hence, it is likely that the dynamic earth pressure acting on the raft side and the structure inertial force acted in the same direction at the times increasing pile stresses, where the absolute value of δ*S* was greater than that of δ*R*.

Figure 21 shows the profiles of the EW relative ground displacements and pile bending moments at $t = t_{Mmax}$ and $t = t_{Mmin}$, together with the maximum and minimum values of the bending moment and displacement. It is seen that the bending moment near the pile head (7B) and those at the intermediate depth in both the piles were close to their maximum at $t = t_{Mmax}$, and the bending moments at the intermediate depth were close to their minimum at $t = t_{Mmin}$ while the bending moment near the pile head (7B) was not close to its minimum. In contrast, the bending moment near the pile toe was very close to its minimum and maximum at $t = t_{Mmax}$ and t_{Mmin}, respectively. At that time the ground displacements both at 1.5 and 15 m depths and the raft displacements were very close to their maximum and minimum. Figure 21 also shows the schematic of foundation deformation and lateral external forces acting on the structure which was supposed based on the monitoring data. Tamura and Hida (2014)

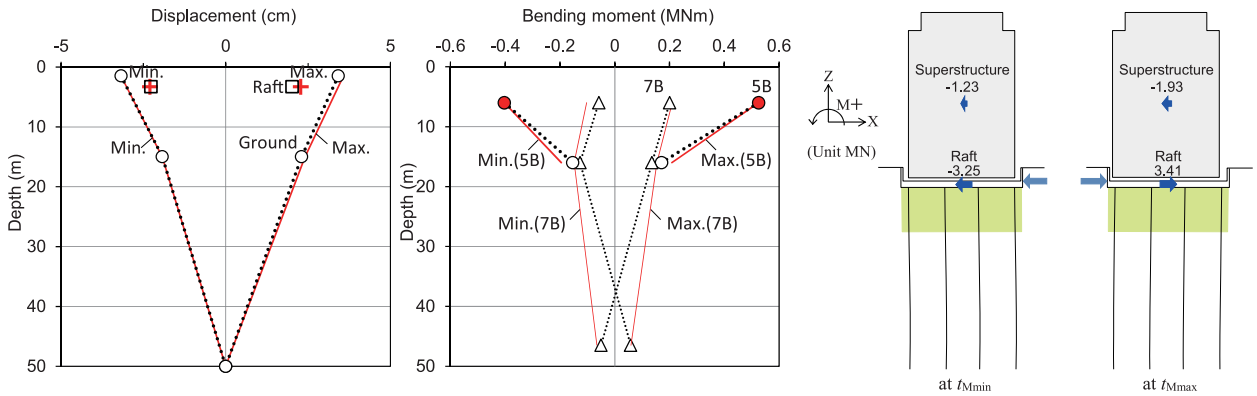

Fig. 21 Profiles of measured ground displacement and pile bending moment at t_{Mmax} and t_{Mmin} (EW)

proposed a method for estimating the phase difference between the structure inertia and earth pressure acting on the raft side. According to the method, if the natural period of the superstructure is greater than predominant period of the ground and δS is greater than δR (which corresponds to the case of the soil-structure system in this paper), the earth pressure tends to be out of phase with the superstructure inertia that is out of phase with the raft inertia. The phase differences illustrated in Fig. 21 are generally consistent with the estimation by the method, while the superstructure inertia was in phase with the raft inertia at $t = t_{Mmin}$.

Consequently, it was found that the maximum bending moments near the pile head, as well as that at the intermediate depth, were affected mainly by the lateral displacements of the thick alluvial silty clay, rather than the shear force resulting from the structure inertial force, as was pointed out in the previous studies (Yamashita et al., 2012; Hamada et al., 2014).

5 SEISMIC PERFORMANCE UNDER STRONG EARTHQUAKES

Shigeno et al. (2017) conducted seismic response analyses of the 12-story building under strong motions using a three-dimensional nonlinear FE model, on the basis of successful numerical simulation of the observation records during the 2011 Tohoku Earthquake. In the study, strong earthquake motions were determined based on Level 2 waves that have been notified in the stipulation of criteria for structural calculations in Japan. A response spectrum of the Level 2 waves is defined in Fig. 22. Figure 22 also shows the response spectra of the base input motions (at 75 m depth) derived from the near surface records during the 2011 Tohoku Earthquake which was used in the numerical simulation of the observation records. In comparison with the Level 2 spectrum, the 2011 earthquake motions would be categorized as a moderate earthquake. In the following, some results of the simulation analysis are presented to discuss the seismic behavior of the piled raft system under strong earthquakes.

Figure 23 shows the profiles of the relative ground displacements at the point A (shown in Fig. 2) and the pile bending moments at $t = t_{Mmax}$ and $t = t_{Mmin}$ under the Level 2 motion of Kobe phase in the NS direction, together with the maximum and minimum values of the bending moment and displacement. Figure 23 also shows the schematic of foundation deformation and external forces acting on the structure. It is seen that the ground displacements and raft displacements at the point A were close to their maximum and minimum. Thus, the maximum bending moments near the pile head were affected mainly by the horizontal ground displacements rather than the shear force resulting from the structure inertial force, as in the same manner as the observation under the moderate earthquake shown in Fig. 21.

Figure 24 shows the relationships between the axial load and the bending moment near the pile head for Piles 5B and 7B observed during the 2011 Tuhoku Earthquake (where the

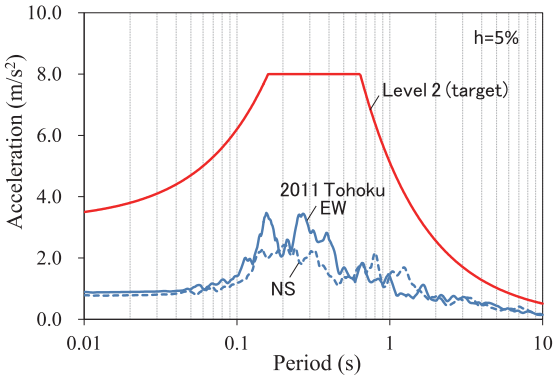

Fig. 22 Acceleration response spectra of Level 2 waves and the 2011 Tohoku Earthquake (75 m depth)

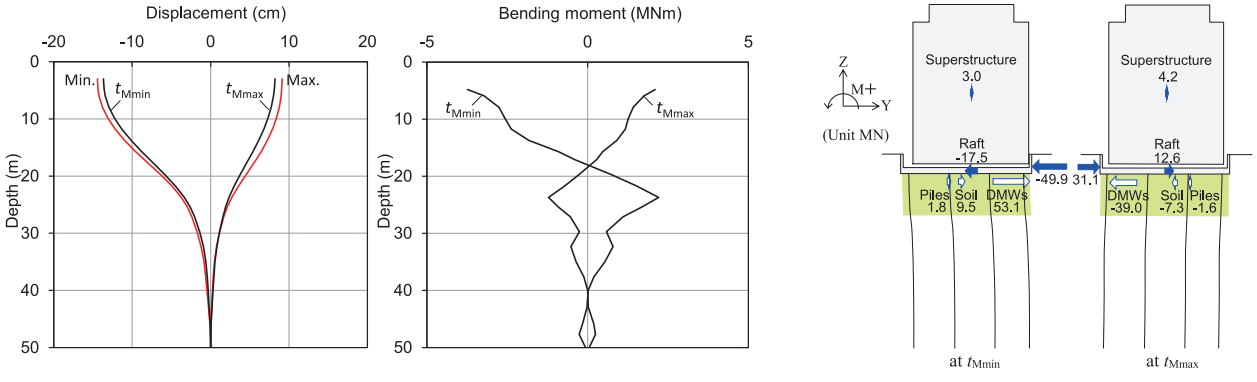

Fig. 23 Profiles of calculated ground displacement at point A and pile bending moment in Pile 5B at t_{Mmax} and t_{Mmin} under Level 2 earthquake (NS)

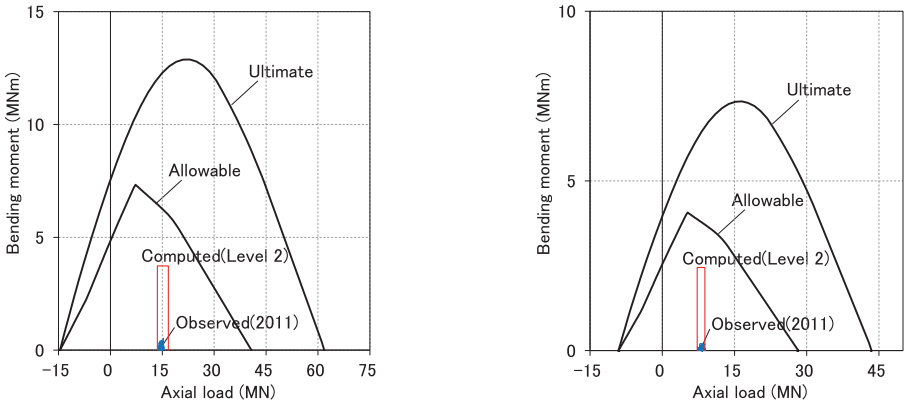

(a) Pile 5B (1.2m dia.) (b) Pile 7B (1.0m dia.)

Fig. 24 Observed and calculated pile bending moments, and design N-M interaction curves

bending moments are obtained by combining the components in NS and EW directions), together with those at the pile head obtained from the numerical simulation under the Level 2 earthquake of Kobe phase. Figure 24 also shows the design interaction curves for the axial load and the bending moment of the SC (steel pipe-concrete composite) pile in Japan which corresponds to the allowable criterion (the unit stress at the edge of the concrete is in the elastic condition) and the ultimate criterion (the unit stress at the edge of the concrete reaches the compressive strength). It is seen that the observed bending moments under the moderate earthquake are very small compared to the allowable criterion. It is also seen that the maximum bending moments under the strong earthquake obtained from the analysis were well below the allowable criterion, while those are more than six times greater than the observed ones under the moderate motion.

6 CONCLUSIONS

Based on the examination of the seismic monitoring data on the soil-pile-structure system recorded during the 2011 Tohoku earthquake, the following conclusions can be drawn:

(1) A peak horizontal ground acceleration of 1.75 m/s^2 was observed near the surface, and the maximum ground displacement near the ground surface (relative to 50 m depth) was 36 mm. No significant changes in foundation settlement or load sharing were observed after the earthquake.

(2) It was found in soft ground that the maximum bending moment near the pile head, as well as that at the intermediate depth, were affected mainly by the lateral displacements of the alluvial silty clay deposit, rather than the shear force resulting from the inertial force from the structure. Furthermore, it was also found that the foundation behavior under strong earthquakes (Level 2 motions) resulted from the previous 3D FE simulation analysis is in the same manner as the observation under the moderate earthquake.

(3) It was found that the DMWs, whose bottom reached relatively stiff clay below the depth of 15.7 m, restrained the amplification of the lateral displacements of soil in the DMW grids. This could be one of reasons for the fact that the bending moments near the pile head were considerably smaller than the allowable criterion in the design. Thus, it is confirmed that a piled raft with grid-form DMWs works effectively in grounds consisting of liquefiable sand and soft cohesive soil.

REFERENCES

Hamada, J., Shigeno, Y., Onimaru, S., Tanikawa, T., Nakamura, N. and Yamashita, K. (2014): Numerical analysis on seismic response of piled raft foundation with ground improvement based on seismic observation records, *Proc. of the 14th Int. Assoc. Computer Methods and Recent Advances in Geomechanics*, 719-724.

Hamada, J., Aso, N., Hanai, A. and Yamashita, K. (2015): Seismic performance of piled raft subjected to unsymmetrical earth pressure based on seismic observation records, *Proc. of the 6th Int. Conf. on Earthquake Geotechnical Engineering*.

Katzenbach, R., Arslan, U. and Moormann, C. (2000): Piled raft foundation projects in Germany, *Design applications of raft*

foundations, Hemsley J.A. Editor, Thomas Telford, 323-392.

Mandolini, A., Russo, G. and Viggiani, C. (2005): Pile foundations: Experimental investigations, analysis and design, *Proc. of the 16th ICSMGE*, Vol. 1, 177-213.

Mendoza, M.J., Romo, M.P., Orozco, M. and Dominguez, L. (2000): Static and seismic behavior of a friction pile-box foundation in Mexico City clay, *Soils & Foundations*, Vol. 40 (4), 143-154.

Poulos, H.G. (2001): Piled raft foundations: design and applications, *Geotechnique*, Vol. 51, No. 2, 95-113.

Poulos, H. G. (2016): Lessons learned from designing high-rise building foundations, *Geotechnical Engineering J. the SEAGS & AGSSEA*, Vol. 47 (4), 35-49.

Shigeno, Y., Yamashita, K. and Hamada, J. (2017): Numerical evaluation of seismic performance of piled raft with grid-form DMWs under large earthquake loads, Proc. of Int. Symposium on design and analysis of piled raft foundations, Taipei, Taiwan.

Tamura, S. and Hida, T. (2014): Pile stress estimation based on seismic deformation method with embedment effects on pile caps, *J. Geotechnical and Geoenvironmental Engineering, ASCE*, Vol. 140, No. 9, 04014049.

Yamashita, K., Yamada, T. and Hamada, J. (2011a): Investigation of settlement and load sharing on piled rafts by monitoring full-scale structures, *Soils & Foundations*, Vol. 51, No. 3, 513-532.

Yamashita, K., Hamada, J. and Yamada, T. (2011b): Field measurements on piled rafts with grid-form deep mixing walls on soft ground, *Geotechnical Engineering J. the SEAGS & AGSSEA*, Vol. 42, No. 2, 1-10.

Yamashita, K., Hamada, J., Onimaru, S. and Higashino, M. (2012): Seismic behavior of piled raft with ground improvement supporting a base-isolated building on soft ground in Tokyo, *Soils & Foundations*, Vol. 52, No. 5, 1000-1015.

Yamashita, K., Hamada, J. and Tanikawa, T. (2016): Static and seismic performance of a friction piled raft combined with grid-form deep mixing walls in soft ground, *Soils & Foundations*, Vol. 56 (3), 559-573.